



**HAL**  
open science

## Generation and characterization of radiolabelled nanosized carbonaceous aerosols for human inhalation studies

Jérémie Pourchez, Iolanda M.D. Albuquerque-Silva, Michèle Cottier, Anthony Clotagatide, Laurent Vecellio, Marc Durand, Francis Dubois

► **To cite this version:**

Jérémie Pourchez, Iolanda M.D. Albuquerque-Silva, Michèle Cottier, Anthony Clotagatide, Laurent Vecellio, et al. Generation and characterization of radiolabelled nanosized carbonaceous aerosols for human inhalation studies. *Journal of Aerosol Science*, 2013, 55, pp.1-11. 10.1016/j.jaerosci.2012.07.011 . hal-00734617

**HAL Id: hal-00734617**

**<https://hal.science/hal-00734617>**

Submitted on 24 Sep 2012

**HAL** is a multi-disciplinary open access archive for the deposit and dissemination of scientific research documents, whether they are published or not. The documents may come from teaching and research institutions in France or abroad, or from public or private research centers.

L'archive ouverte pluridisciplinaire **HAL**, est destinée au dépôt et à la diffusion de documents scientifiques de niveau recherche, publiés ou non, émanant des établissements d'enseignement et de recherche français ou étrangers, des laboratoires publics ou privés.

**Generation and characterization of radiolabelled nanosized carbonaceous  
aerosols for human inhalation studies**

Jérémy Pourchez<sup>a,b,c</sup>, Iolanda M. D. Albuquerque-Silva<sup>a,b,c</sup>, Michèle Cottier<sup>a,c,d,e,f</sup>,  
Anthony Clotagatide<sup>e</sup>, Laurent Vecellio<sup>g,h</sup>, Marc Durand<sup>a,c,i</sup>, Francis Dubois<sup>a,c,d,e,f</sup>

<sup>a</sup> LINA, EA 4623, F-42023, Saint-Etienne, France

<sup>b</sup> Ecole Nationale Supérieure des Mines de Saint-Etienne, Centre Ingénierie et Santé, F-42023, Saint-Etienne, France

<sup>c</sup> SFR IFRESIS, F-42023, Saint-Etienne, France

<sup>d</sup> Université Jean Monnet, Faculté de Médecine, F-42023, Saint-Etienne, France

<sup>e</sup> CHU de Saint-Etienne, F-42055, Saint-Priest en Jarez, France

<sup>f</sup> Université de Lyon, F-42023, Saint-Etienne, France

<sup>g</sup> DTF Aerodrug – Diffusion Technique Française, Tours, France

<sup>h</sup> INSERM U1100-EA6305, Université François Rabelais, Tours, France

<sup>i</sup> Centre Hospitalier Emile Roux, F-43012, Le Puy en Velay, France

Correspondence to: Jérémy POURCHEZ, Ecole Nationale Supérieure des Mines de Saint-Etienne, Centre Ingénierie et Santé, 158 Cours Fauriel 42230, France.  
Telephone / Fax number: + 33 4 77 42 01 80 / +33 4 77 49 96 94, mail:  
pourchez@emse.fr

2 **ABSTRACT**

3 New insights on the output of a commercial Technegas generator were proposed in  
4 order to optimize the generation of a radioactive nanosized aerosol for human  
5 inhalation studies. Parameters influencing Technegas generated aerosols (*i.e.*  
6 gaseous atmosphere, generation temperature and storage duration) were analyzed  
7 by a combination of size-fractionation and gamma-scintigraphy detection to  
8 determine the aerosol aerodynamic-related distributions. It was found that the total  
9 radioactivity per mass and number concentrations of aerosols was mostly influenced  
10 by the burn temperature, while the radiolabelling of particles was mostly driven by  
11 their surface area. <sup>99m</sup>Tc labeled nanosized carbonaceous primary particles appear  
12 mainly to result from nucleation/condensation of the supersaturated vapor during the  
13 burning step, and then coalesce into larger particles due to coagulation processes  
14 during the residence time in the expansion chamber. We showed that the burn  
15 temperature and the aerosol residence time were the main parameters influencing  
16 the particle size distribution. Under optimized operating conditions, the amount of  
17 radiolabelled nanoparticles substantially increased since the radioactivity median  
18 aerodynamic diameter was reduced by half (250 nm - GSD of 2.5) compared with the  
19 standard operating conditions of the Technegas generator (450 nm - GSD of 3.4).

20

21 **KEYWORDS:** Technegas; ELPI; radiolabelled nanosized aerosols

22

23 **MAIN TEXT**

24 **1. Introduction**

25 Radiolabelled aerosols are widely used to study airborne particle deposition patterns  
26 in the lung as well as lung clearance (Möller et al., 2006; Sanchez-Crespo et al.,  
27 2011; Carvalho et al., 2011). Among all the radiolabelled aerosols clinically used in  
28 patients, one of the most convenient is the “Technegas technique” widely used to  
29 perform lung ventilation scintigraphy as a diagnostic technique in nuclear medicine.  
30 The aerosol produced is commonly known as Technegas, an ultrafine suspension of  
31 carbon particles labeled with technetium ( $^{99m}\text{Tc}$ ). Technegas preparation takes place  
32 in a specially designed machine, called the Technegas generator, where a solution of  
33 sodium pertechnetate is loaded into a graphite crucible and evaporated until dry.  
34 Technegas is then generated by heating to 2550 °C in an atmosphere of pure argon.  
35 The number size distribution of Technegas particles is mainly below 100 nm (Vita  
36 Medical Ltd., 2000). Since more than 2 decades, this radioactive aerosol is regularly  
37 used as a ventilation scintigraphy agent, and the device is approved for human  
38 application without any toxicological issues (Jögi et al., 2010, Senden et al., 1997;  
39 Lloyd et al., 1995; Burch et al., 1986). Due to the short half-life of  $^{99m}\text{Tc}$  (6.02 h), the  
40 radiation dose can be kept low (< 0.1 mSv) even though the resulting high activities  
41 allow high quality gamma-camera imaging in nuclear medicine.

42 Under standard operating conditions, the Technegas generator produces airborne  
43 particles with leaching rates >10% which are too high for clearance studies. Since  
44 NaCl contained in the  $^{99m}\text{Tc}$ -eluate also evaporates and condenses during the  
45 burning step, the particles have hygroscopic properties and the radiolabel leaches  
46 from them. Recently Moeller et al. (2006) proposed several modifications to the  
47 operating conditions of the Technegas generator to avoid these drawbacks such as

48 the use of NaCl free  $^{99m}\text{Tc}$ -eluate. In addition the particles could be labeled by  $^{111}\text{In}$   
49 (Sanchez-Crespo et al., 2011) or  $^{68}\text{GaCl}_3$  (Borges et al., 2011) instead of  $^{99m}\text{Tc}$  to  
50 extend the investigation time of clearance studies from 1 day to a few weeks.

51 Although it is generally accepted that the Technegas generator produces a  
52 smaller particle size than other conventional radiolabelled aerosols, few data are  
53 available about its particle size characteristics. To the best of our knowledge no data  
54 have yet been reported on the relationship between radioactivity aerodynamic  
55 diameter (AMAD) although this parameter is crucial to assess deposition patterns.  
56 Even the median diameter remains poorly defined in the range from about 200 to 400  
57 nm (Borges et al. 2011, Lemb et al., 1993; Strong and Agnew, 1989; Möller et al.,  
58 2006). In fact, clinical experiments in nuclear medicine indicate that radiolabelled  
59 Technegas particles are likely to impact on obstructions within the respiratory tract,  
60 which is a behavior typically attributed to micrometer sized aerosols (Jögi et al.,  
61 2010).

62 The radiolabelling mechanism and radiolabelling efficiency of airborne particles  
63 related to their aerodynamic size also remain poorly understood. Therefore, this  
64 study aims at new insights on the output of a Technegas device generating  $^{99m}\text{Tc}$   
65 labeled nanosized carbonaceous aerosols. The physical properties of the airborne  
66 nanoparticles in term of radiolabelling efficiency, number, mass and surface area  
67 concentrations are characterized by using a combination of size-fractionation and  
68 gamma-scintigraphy detection. Based on the experimental methodology previously  
69 developed by Moeller *et al.* (2006), we also propose a better understanding of the  
70 effect of Technegas generator operating conditions on the characteristics of the  
71 radiolabelled particle size distributions. Finally, we also describe optimal operating  
72 conditions to generate radiolabelled carbonaceous nanoparticles.

## 73 **2. Material and methods**

74 The generation of Technegas was first reported in 1986, as a simple process  
75 consisting of evaporating Technetium ( $^{99m}\text{Tc}$ ) containing eluate in a graphite crucible  
76 at 2500°C (Burch et al., 1986). The Technegas generator is essentially a miniature  
77 high temperature furnace (Figure 1). It uses a combination of graphite in an argon  
78 atmosphere to chemically reduce the pertechnetate ion  $\text{TcO}_4^-$  contained in the  $^{99m}\text{Tc}$   
79 sodium pertechnetate solution to metallic technetium (Tc), and then produce metallic  
80 aerosol particles by vaporizing both carbon and technetium elements. The inert  
81 atmosphere is critical to produce pure carbon or metallic aerosols (Evans et al.,  
82 2003). The crucible is the source of graphite vapour which ultimately coats the  
83 technetium metal. An AC electrical current passes through two conducting substrates  
84 (electrodes and crucible) possessing relatively low vapour pressure. The metallic  
85 aerosol forms first by nucleation/condensation of the vapour, followed by  
86 agglomeration of airborne nanoparticles composed of hexagonal platelets of metallic  
87 technetium ( $^{99m}\text{Tc}$ ) closely encapsulated with a thin layer of graphitic carbon. During  
88 Technegas production, particles are not equally radiolabelled. The rapid volatilization  
89 of the species involved and the surface passivation of the resulting metallic aerosol  
90 are major factors influencing particles formation and stabilization, which may proceed  
91 differently according to particle size distribution (Senden et al., 1997).

92 In this work, the Technegas generator (Cyclomedica Pty Ltd, Australia) was  
93 operated in its “maintenance mode”, which allows modifying its operating conditions.  
94 A pyrometer was coupled to the generator in order to control burn temperature. For  
95 aerosol production, a standard graphite crucible was previously humidified with 99%  
96 ethanol in order to increase its wettability and then filled with a 200MBq  $^{99m}\text{Tc}$ -sodium  
97 pertechnetate solution placed in the Technegas generator chamber. The produced

98 aerosol was subsequently analyzed by an electrical low pressure impactor (ELPI,  
99 Dekati Ltd., Finland) and a gamma camera (Millenium, GE, USA), to determine the  
100 particle size distribution both by weight, number, surface area and radioactivity. The  
101 NaCl content in <sup>99m</sup>Tc-eluate was also evaluated with respect to its influence on the  
102 final particle size distribution. All experiments were performed in triplicate and  
103 statistically analyzed (unpaired t-test).

104

### 105 *2.1 Aerosol generation parameters*

106 Under standard clinical operating conditions, the aerosol production is initiated  
107 through the “*simmer*” stage, which is characterized by a modification of the generator  
108 chamber atmosphere by argon flushing and a slight heating of the crucible up to  
109 80°C for a 6 minute duration (Vita Medical Ltd., 2000). Under these conditions, the  
110 <sup>99m</sup>Tc eluate is evaporated to dryness, providing an intimate contact between the  
111 crucible and the species of <sup>99m</sup>Tc-sodium pertechnetate solution (Senden et al.,  
112 1997). Subsequently, the “*burn*” stage begins in which the crucible is finally heated to  
113 2550°C for 10 seconds (Vita Medical Ltd., 2000). This heating leads to technetium  
114 and carbon evaporation with subsequent condensation and aerosol formation. It is  
115 therefore reasonable to conclude that the major parameters influencing aerosol  
116 generation are the burn temperature, the duration of the simmer and the burn stages.  
117 Another important parameter is the residence time in the expansion chamber. During  
118 clinical procedures, a delay (*i.e.* a residence time in the expansion chamber) occurs  
119 between Technegas generation and its delivery to the patient. This delay is usually  
120 on the order of 2 minutes. During the residence time in the expansion chamber,  
121 particles are able to coagulate and agglomerate, with a significant impact on the

122 subsequent size distribution of the radioactive aerosol delivery to the patient (Möller  
123 et al., 2006).

124 The standard clinical parameters for Technegas production are prescribed as 6  
125 minutes of simmering, followed by 10 s of burning at 2500°C followed by 2 minutes of  
126 residence time. However, in order to reduce the consumption of the generator  
127 electrodes, in this work the standard burn stage duration was reduced to 5 seconds  
128 instead of 10. The proposed change of operating conditions of the Technegas  
129 generator was based on a previous study from Möller et al. (2006). The analyses of  
130 particle size distribution were performed by varying each generation parameter: (I)  
131 simmer duration (6 – 15 min); (II) burn temperature (1900 – 2800°C); (III) burn  
132 duration (2 – 15s) and (IV) aerosol residence time (0.5 – 10 min). The operating  
133 conditions of the Technegas generator were summarized in Figure 2.

134

## 135 *2.2 Particle size distributions*

136 Aerosol size distributions were determined using the ELPI low pressure impactor.  
137 The ELPI classifies by aerodynamic diameter, in 12 size fractions ranging from 10  
138 µm to 7 nm (Virtanen et al., 2001; Marjamäki et al., 2000). The number concentration  
139 was converted to mass and surface area concentrations assuming the graphite  
140 crucible density ( $2.13 \text{ g.cm}^{-3}$ ) for the particles. Differential distributions and  
141 normalized cumulative distributions are shown in accordance with the European  
142 standard EN 13544-1 for respiratory therapy equipment, which is widely employed for  
143 pharmaceutical aerosols. The cumulative distributions were normalized, *i.e.* data  
144 were expressed in % where 100% corresponds to total radioactivity (from gamma-  
145 camera measurements) or total mass/number/surface area (from ELPI calculations)  
146 deposited on all the 12 collection plates of the cascade impactor.



147 *2.3 Radioactivity measurements*

148 A combination of ELPI size fractionation and gamma scintigraphy detection  
149 was used to determine the aerodynamic radioactivity size distribution. For this  
150 purpose, the aerosol was collected on cellulose substrates inserted on the collection  
151 plates of the impactor. The radioactivity of airborne particles deposited on each  
152 collection substrate was determined by gamma scintigraphy imaging during a 2  
153 minutes acquisition time. The distribution of radioactivity is presented versus the ELPI  
154 stage mid-point aerodynamic diameter.

155

156 *2.4 Electron microscopy observations and chemical analysis*

157 Field Emission Gun Scanning Electron Microscopy (FEG SEM, Jeol JSM  
158 6500F) was used to analyze the Technegas particles deposited within the ELPI  
159 stages. SEM observations coupled with image analysis also provided a mean  
160 geometric particle diameter for each size class of the ELPI.

161 The sodium and chloride concentrations in the Tc-eluate were obtained by ion  
162 chromatography with a Dionex apparatus composed of a GP50 pump, a CS12A  
163 column for cation analysis, a AS11HC column for anions, a CD conductometric  
164 detector and a UV-visible detector. The presence of NaCl in the airborne particles  
165 was characterized using energy-dispersive X-ray spectroscopy (EDX) coupled with a  
166 scanning electron microscope. The EDX analytical technique was used for the  
167 elemental analysis of airborne particles (except carbon and technetium elemental  
168 detection). The sodium, chloride and technetium content of airborne particles were  
169 measured using X-ray photoelectron spectroscopy (XPS). XPS is a quantitative  
170 spectroscopic technique for the elemental composition.

171

### 172 **3. Results**

#### 173 *3.1 Technegas aerosol under standard operating conditions*

174 A linear correlation was found between the geometric diameter of particles  
175 calculated by image analysis from SEM images and the corresponding mid-point  
176 aerodynamic diameter of the ELPI stage (Figure 3). Results show a particle  
177 distribution composed of a predominantly carbonaceous nature for the ultrafines  
178 particles (in the 30-300 nm size range) and the dominant NaCl content of the micron  
179 sized particles (Figure 3). The sodium chloride content of numerous micrometer sized  
180 particles was clearly put in evidence by EDX spectroscopy during SEM observations  
181 and XPS analysis. On the ELPI stages corresponding to mid-point aerodynamic  
182 diameters higher than 1  $\mu\text{m}$ , SEM images also show the presence of coagulated  
183 carbonaceous particles (data not shown but similar to Figure 7), which precluded the  
184 correct determination of their geometric diameter, leading to slight deviations from  
185 ELPI measurements even if the overall correlation remains quite good.

186 The particle size distributions of the aerosol obtained under standard operating  
187 conditions used in clinical routine are first presented in terms of number, surface  
188 area, mass and radioactivity (Figure 4). Number distributions are dominated by  
189 nanoparticles with aerodynamic diameters lower than 100 nm with a Count Median  
190 Aerodynamic Diameter (CMAD) of 40 nm (GSD of 2.9). However, radioactivity  
191 distributions indicate that radiolabelled particles are mostly distributed in the range  
192 between 100 nm and 1  $\mu\text{m}$ , providing an Activity Median Aerodynamic Diameter  
193 (AMAD) of 450 nm (GSD of 3.4). Radioactivity distributions were found to be in good  
194 accordance with surface area distributions, characterized by a Surface Median  
195 Aerodynamic Diameter (SMAD) of 540 nm (GSD of 2.1). Finally, mass distributions

196 showed particles exclusively distributed in the size range above 100 nm, leading to a  
197 Mass Median Aerodynamic Diameter (MMAD) of 820 nm (GSD of 2.7) .

198 The combination of aerodynamic and radioactivity measurements provides new  
199 insights into the radiolabelling process. A radiolabelling efficiency was defined as the  
200 ratio between activity (in fact radioactivity, in Bq) and mass from particles deposited  
201 on each ELPI stage. According to Figure 5, particle radiolabelling is most efficient in  
202 the nanometer range and then decreases continuously with aerodynamic diameter.

203 The electric charge level of the freshly generated airborne Technegas particles  
204 was also checked by ELPI (using the ELPI with the corona charger OFF) in order to  
205 verify that the original electric charge of the particles does not affect the ELPI  
206 detection based on current measurement. Results show that the aerosol particles are  
207 weakly charged and that the charge distribution depends to the aerodynamic particle  
208 size. Particles are positively charged (13 fC) for sizes from 28 to 262 nm, negatively  
209 charged (-12 fC) in the range 262 nm to 1.6  $\mu\text{m}$ , and finally neutral for sizes greater  
210 than 1.6  $\mu\text{m}$ . In this case, the corona charger produces a sufficient amount of positive  
211 ions to first neutralize and then charge the particles normally up to 7500 fC, 500  
212 times higher than the original electric charge of the particles. Furthermore, the use of  
213 cellulose substrates for particles recovery on the ELPI stages has no significant  
214 influence ( $p < 0.05$ ) on the Technegas particle size distribution. Both methods  
215 generate aerosol with an AMAD of 445 (GSD of 3.0) and 450 nm (GSD of 2.7)  
216 respectively (Table 1).

217

### 218 *3.2 Technegas aerosol characteristics under modified operating conditions*

219 We now show that the modified operating conditions significantly influence the  
220 particle size distribution (Figure 6). Results are also summarized as mean of AMAD

221 and GSD in Table 2. An increased simmer increases the amount of nanoparticles  
222 significantly. 15 minutes of simmering (instead of 6 min under standard clinical  
223 operating conditions) increase the nanoparticle population by 10%, leading to a  
224 reduction of the Technegas AMAD from 450 to 305 nm. Increasing the burn duration  
225 from 2 to 10 seconds also reduces the AMAD from 500 to 370 nm. However,  
226 increasing the burn duration beyond 10 seconds does not have a significant influence  
227 on the aerosol AMAD.

228 The burn temperature of the crucible, and the aerosol residence time in the  
229 expansion chamber, appear to be the main parameters affecting aerosol generation.  
230 Therefore, either an increase of burn temperature or a decrease of residence time  
231 leads to a substantial reduction of aerosol AMAD and an increased amount of  
232 radiolabelled nanoparticles. Increasing the burn temperature from 1900°C to 2800°C  
233 leads to a decrease of AMAD from 510 to 270 nm. A decrease of residence time from  
234 10 minutes to 0.5 minutes gave a decrease of AMAD from 540 to 285 nm. SEM  
235 observations showed that the morphology of aerosols particles was also highly  
236 dependent on their residence time. Therefore, particle coagulation and agglomeration  
237 were visibly reduced for small aerosol residence times (30 seconds) but manifestly  
238 present for long residence times (10 minutes) (Figure 7).

239 Moreover, the total amount of aerosol radioactivity, *i.e.* the number of technetium  
240 atoms fixed on carbonaceous particles, was also strongly influenced by the  
241 generation parameters, especially by the burn temperature (Figure 8). Thus, a  
242 reduction of temperature to 1900°C causes a significant reduction in total  
243 radioactivity, up to 4 times lower than in standard clinical operating conditions.

244 Finally, the radiolabelled particle size was mostly affected by the burn  
245 temperature. Thus, an optimization of the generation method is proposed based on

246 adjustments of the burn temperature, in order to maximize the production of  
247 radiolabelled nanoparticles. This optimized method of radiolabelled aerosol  
248 production was performed by two consecutive burn stages, using both extremes of  
249 burn temperature of the generator: 5 second burn at 1900°C followed by 5 second  
250 burn at 2800°C. The optimized radiolabelled aerosol showed an aerodynamic particle  
251 size distribution with an AMAD of 250 nm (GSD of 2.5), about 2 times smaller than  
252 standard Technegas, but to a 15% increase of the radiolabelled nanoparticles (Figure  
253 9).

254       Once the optimized conditions for Technegas production were determined, the  
255 influence of the NaCl content on Tc-eluate was analyzed. Ionic chromatography  
256 confirms the very low NaCl concentration (in the range 20-100 mg/L) of the NaCl free  
257 Tc-eluate, by comparison with the NaCl concentration of 9 g/L for NaCl Tc eluate.  
258 Results further prove that an initially NaCl-free eluate did not significantly modify the  
259 particle size distribution (AMAD of 200 nm) (Figure 9).

260

#### 261 4. Discussion

262 In the present study, based on a methodology combining radioactivity  
263 measurements and aerodynamic size fractionation, for the first time the Technegas  
264 size distributions are expressed in terms of size-related radioactivity, characterized  
265 by AMAD. Using ELPI based calculations, the aerosol was also characterized by its  
266 CMAD, SMAD and MMAD. These calculations are based on positive ion active  
267 surface areas measured by ELPI, and the masses of spheres with diameter equal to  
268 the midpoint aerodynamic values ( $D_a$ ) of each stage. Active surface area is generally  
269 defined as the surface of a particle that is involved in interactions with the  
270 surrounding gas (Fuchs, 1963). Thus, the ELPI provides a real time size-selective  
271 (aerodynamic diameter) active surface-area concentration. In this sense the surface  
272 area measured by the ELPI is an active surface area quite relevant to describe Tc-  
273 carbone interactions. The active surface area distribution appears to be the most  
274 appropriate form to describe the radiolabelled particles distributions since a good  
275 correlation is observed between surface area and radioactivity cumulative  
276 distributions (Figure 4). This original data demonstrates that particle radiolabelling is  
277 mostly proportional to their active surface area, rather than particle number or mass.  
278 In other words, the quantity of technetium atoms fixed on the carbonaceous particles  
279 is mainly dependent to their active surface area.

280 Further, the Technegas MMAD (820, GSD of 2.7) was found to be almost 20  
281 times higher than its CMAD, which trivially indicates that Technegas nanoparticles,  
282 although abundant in number, are not significant in mass. However, activity  
283 measurements provide an AMAD (450 nm, GSD of 3.4) corresponding to the half of  
284 Technegas MMAD, which can be explained by the fact that its nanoparticles,  
285 although insignificant in mass, have a considerable radioactivity. The radiolabelling

286 efficiency of Technegas particles, expressed by means of activity-to-mass ratio, also  
287 indicates that particle radiolabelling was more efficient on the nanometric scale  
288 (Figure 5). This result highlights the role played by particle surface area during  
289 radiolabelling. In this sense, the higher active surface area to volume ratio of  
290 nanoparticles (compared to micrometric particles) can easily explain the continuous  
291 decrease of radioactivity to mass ratio with the increase of aerodynamic diameter.  
292 The remarkable radiolabelling efficiency of nanoparticles can also be explained by  
293 their mode of production. In previous work, Senden et al. (1997) observed that the  
294 radioactivity only leaves the crucible at the melting point for technetium ( $2250 \pm$   
295  $50^\circ\text{C}$ ), which probably indicates that there is a passive mechanism of particle ejection  
296 from the crucible (i.e. the evaporation of the metal). Once in the vapor phase,  
297 technetium may condense as a metallic aerosol, being instantly passivated by  
298 condensed carbon (Senden et al., 1997).

299 Our data support the assumption that the generation of Technegas nanoparticles  
300 is driven by a mechanism quite similar to aerosol produced by spark discharge  
301 generators. Technegas nanoparticle generation could be therefore explained by a  
302 simultaneous ablation of technetium and graphite, caused by the striking of an  
303 alternative current arc from the thermionic plasma inside the crucible (Vita Medical  
304 Ltd., 2000).  $^{99\text{m}}\text{Tc}$  labeled nanosized carbonaceous particles appear mainly to result  
305 from nucleation/condensation during the burning step followed by coagulation  
306 processes during the residence time in the expansion chamber. Nevertheless, these  
307 mechanisms are still not entirely proven and require further investigations.

308 All the operating conditions of the Technegas generator (i.e. simmer, burn duration,  
309 burn temperature and aerosol residence time) show an influence on the particle size  
310 distribution (Figure 6). A decrease of aerosols AMAD was observed with increasing

311 simmer and burn durations. These parameters apparently facilitate ablation and  
312 condensation phenomena and thus contribute to the AMAD reduction. Although the  
313 simmer and burn duration had some impact on the particle size distribution, stronger  
314 modifications were observed by adjusting on the residence duration in the expansion  
315 chamber and the burn temperature. Longer residence times obviously lead to  
316 coagulation and a higher AMAD (Table 2, Figure 7). This result confirms the relative  
317 instability of freshly radiolabelled nanoparticles over the timeshown in previous  
318 studies (Llyod et al.,1995, Möller et al., 2006). A noticeable reduction of AMAD from  
319 510 nm (GSD of 3.0) to 270 nm (GSD of 2.7) was observed for an increase of burn  
320 temperature from1900°C to 2800°C. Furthermore, burn temperature was the  
321 parameter which had the strongest influence on the total aerosol radioactivity (Figure  
322 8). As the burn temperature plays a major role on the output of Technegas device, an  
323 optimized method has been proposed which is based on a temperature of 1900°C  
324 followed by 2800°C to reduce the AMAD (Figure 9).

325 Finally, we demonstrate that the absence of sodium chloride in the initial  
326 pertechnetate eluate does not significantly modify the particle size distribution (AMAD  
327 of 200 nm) compared to usual NaCl pertechnetate eluate (Figure 9). This result  
328 suggests that NaCl crystals generated using NaCl Tc-eluate are poorly radiolabelled  
329 compared to carbonaceous nanoparticles. Previous studies (Moller et al., 2006,  
330 Wiebert et al., 2006a, 2006b) demonstrated that the removal of NaCl from <sup>99m</sup>Tc-  
331 sodium pertechnetate also yielded low leaching rates of radiolabel from particles of  
332 below 4% within 24h, and also guaranteed non-hygroscopic aerosol properties. The  
333 removal of NaCl from the Tc-eluate therefore seems to have several advantages.

334



335 **Conclusion**

336 The particle size distribution of the Technegas generator has been characterized  
337 from combined measurements of radioactivity (using a gamma camera) and  
338 aerodynamic sizing (using ELPI). Under standard clinical operating conditions,  
339 Technegas shows a radioactivity median aerodynamic diameter (AMAD) of 450 nm  
340 (GSD of 3.4). The particle size distribution and the total radioactivity of the aerosol  
341 are mostly influenced by the burn temperature. We proposed an optimized procedure  
342 to produce radiolabelled nanoparticles using the commercial Technegas generator  
343 consisting of two consecutive burns at 1900°C and 2800°C. Under optimized  
344 conditions, the median diameter of Technegas can thereby be reduced by half (250  
345 nm), together with a substantial increase of its radiolabelled nanoparticle population.

346 Aerosols containing a greater amount of radiolabelled nanoparticles may permit  
347 better particle deposition within the respiratory tract. In this context an improvement  
348 of lung ventilation scintigraphy in nuclear medicine is conceivable. These new  
349 insights appear also valuable to assess deposition patterns of well-defined  
350 nanoparticles within the respiratory tract, in the case of inhalation toxicology and drug  
351 delivery by aerosol therapies. Finally, the proposed approach to optimize the  
352 generation of radioactive nanosized aerosol using the technegas generator can be  
353 coupled with other previous modifications such as a higher stable radiolabelling over  
354 time by removing NaCl from the Tc-eluate, or the possibility of  $^{111}\text{In}/^{68}\text{GaCl}_3$   
355 labelling, to enhance alveolar pattern deposition and provide potential clinical  
356 improvements on inhalation studies.

357

358 **ACKNOWLEDGEMENTS**

359           The authors would like to acknowledge the financial support of the Regional  
360 French Association for Aid to Chronic Respiratory Failure Patients (ARAIR), Saint-  
361 Etienne Métropole and the Conseil Général de la Loire, as well as the helpful  
362 conversations and experimental support of the Cyclopharma Laboratoires (France).  
363 The authors would like also to thank the editor for all corrections and helpful  
364 comments which greatly contribute to this paper. Finally, special thanks to Laurent  
365 Navarro (Ecole Nationale Supérieure des Mines de Saint-Etienne, Centre Ingénierie  
366 et Santé, France) for his contribution to the image analysis and algorithm  
367 development on SEM images.

368

369           **REFERENCES**

370   Borges, J.B., Velikyan, I., Langström, B., Sörensen, J., Ulin, J., Maripuu, E.,  
371   Sandström, M., Widström, C., Hedenstierna, G. (2011). Ventilation distribution  
372   studies comparing Technegas and “Gallgas” using  $^{68}\text{GaCl}_3$  as the label. *Journal of*  
373   *Nuclear Medicine*, 52, 206-209.

374

375   Burch, W.M., Sullivan, P.J., McLaren, C. (1986). Technegas – a new ventilation  
376   agent for lung scanning. *Nuclear Medicine Communications*, 7, 865-871.

377

378   Carvalho, T.C., Peters, J.I., and Williams, R.O. (2011) Influence of particle size on  
379   regional lung deposition – What evidence is there? *International Journal of*  
380   *Pharmaceutics*, 406, 1-10.

381

382   Dekati Ltd. ELPI in pharmaceutical measurements. In: Dekati Ltd Application Note.  
383   2007.

384

385   Evans, D.E., Harrison, R.M., Ayres J.G. (2003). The generation and characterization  
386   of elemental carbon aerosols for human challenge studies. *Journal of Aerosol*  
387   *Science*, 34, 1023-1041.

388

389   Fuchs, N. (1963) On the stationary charge distribution on aerosol particles in a  
390   bipolar ionic atmosphere. *Geofisica Pura e Applicata*, 56, 185-193.

391

392 Jögi, J., Jonson, B., Ekberg, M., Bajac, M. (2010). Ventilation-Perfusion SPECT with  
393 <sup>99m</sup>Tc-DTPA versus Technegas: A head-to-head study in obstructive and  
394 nonobstructive disease. *Journal of Nuclear Medicine*, 51, 735-741  
395

396 Lemb, M., Oei, T.H., Eifert, H., Günther, B. (1993). Technegas: a study of particle  
397 structure, size and distribution. *European Journal of Nuclear Medicine*, 20, 576-579.  
398

399 Lloyd, J.J., Shields, R.A., Taylor, C.J., Lawson, R.S., James, J.M., Testra, H.J.  
400 (1995). Technegas and Pertechnegas particle size distribution. *European Journal of*  
401 *Nuclear Medicine*, 22, 437-476  
402

403 Marjamäki, M., Keskinen, J., Chen, D.R., Pui, D.Y.H. (2000). Performance evaluation  
404 of the electrical low-pressure impactor (ELPI). *Journal of Aerosol Science*, 31, 249-  
405 261.  
406

407 Möller, W., Felten, K., Seitz, J., Sommerer, K., Takenaka, S., Wiebert, P., Philipson,  
408 K., Svartengren, M., Kreyling, W.G. (2006). A generator for the production of  
409 radiolabelled ultrafine carbonaceous particles for deposition and clearance studies in  
410 the respiratory tract. *Journal of Aerosol Science*, 37, 631-644.  
411

412 Sanchez-Crespo, A., Klepczynska-Nyström, A., Lundin, A., Larsson, B.M.  
413 Svartengren, M. (2011). Indium-labeled ultrafine carbon particles; a novel aerosol for  
414 pulmonary deposition and retention studies. *Inhalation Toxicology*, 23, 121-128.  
415

416 Senden, T.J., Moock, K.H., Gerald, J.F., Burch, W.M., Browitt, R.J., Ling, C.D., and  
417 Heath, G.A. (1997). The physical chemical nature of Technegas. *Journal of Nuclear*  
418 *Medicine*, 38, 1327-1333.

419

420 Strong, J.C., Agnew, J.E. (1989). The particle size distribution of Technegas and its  
421 influence on regional lung deposition. *Nuclear Medicine Communications*, 10, 425-  
422 430.

423

424 Virtanen, A., Marjamäki, M., Ristimäki, J., Keskinen, J. (2001). Fine particle losses in  
425 electrical low-pressure impactor. *Journal of Aerosol Science*, 32, 389-401.

426

427 Vita Medical Ltd. Technegas Service Manual Document N°70305. 2000:P2-4.

428

429 Wiebert P., Sanchez-Crespo A., Falk R., Philipson K., Lundin A., Larsson S., et al.  
430 (2006a). No significant translocation of inhaled 35-nm carbon particles to the  
431 circulation in humans *Inhalation Toxicology* 18, 741–747.

432

433 Wiebert, P., Sanchez-Crespo, A., Seitz, J., Falk, R., Philipson, K., Kreyling, W. G.,  
434 Moller, W., Sommerer, K., Larsson, S., and Svartengren, M. (2006b). Negligible  
435 clearance of ultrafine particles retained in healthy and affected human lungs.  
436 *European Respiratory Journal*, 28, 286-290.

437

438

439

440 **TABLES LEGENDS**

441 **TABLE 1.** Influence of generator mode and ELPI collection substrates on aerosols  
442 particle size distributions: radioactivity median aerodynamic diameters (AMAD) and  
443 geometric standard deviation (GSD).

444 **TABLE 2.** Radioactivity median aerodynamic diameters (AMAD) and geometric  
445 standard deviation (GSD) under standard clinical operating conditions, or under  
446 modified and optimized operating conditions (modified generation parameters in  
447 bold).

448

449

450 **FIGURES LEGENDS**

451 **FIGURE 1.** Schematic diagram of the Technegas generator.

452 **FIGURE 2.** Operating conditions of the Technegas generator: description of analyzed  
453 parameters.

454 **FIGURE 3.** EDX analysis coupled with SEM observation of ELPI stage showing  
455 carbonaceous nanoparticles (A) and NaCl crystals (B). Linear correlation between  
456 geometric diameter obtained by image analysis on SEM images and corresponding  
457 mid-point aerodynamic diameter determined by ELPI.

458 **FIGURE 4.** Aerodynamic size distributions of aerosol generated under standard  
459 clinical operating mode: differential distributions from ELPI calculations (top) and  
460 cumulative distributions from combined ELPI and gamma-camera measurements  
461 (bottom).**FIGURE 5.** Radiolabelling efficiency expressed as radioactivity per mass of  
462 particle.

463 **FIGURE 5.** Radiolabelling efficiency expressed as activity per particle mass.

464 **FIGURE 6.** Operating parameters influencing Technegas aerodynamic particle size  
465 distribution. Clinical operating conditions are used as a reference (distribution in black  
466 bold line).

467 **FIGURE 7.** SEM images of particles deposited on ELPI stage corresponding to mid-  
468 point aerodynamic diameter of 2.39  $\mu\text{m}$  for residence times of (A) 30 seconds and (B)  
469 10 minutes. Arrows indicate agglomerated particles.

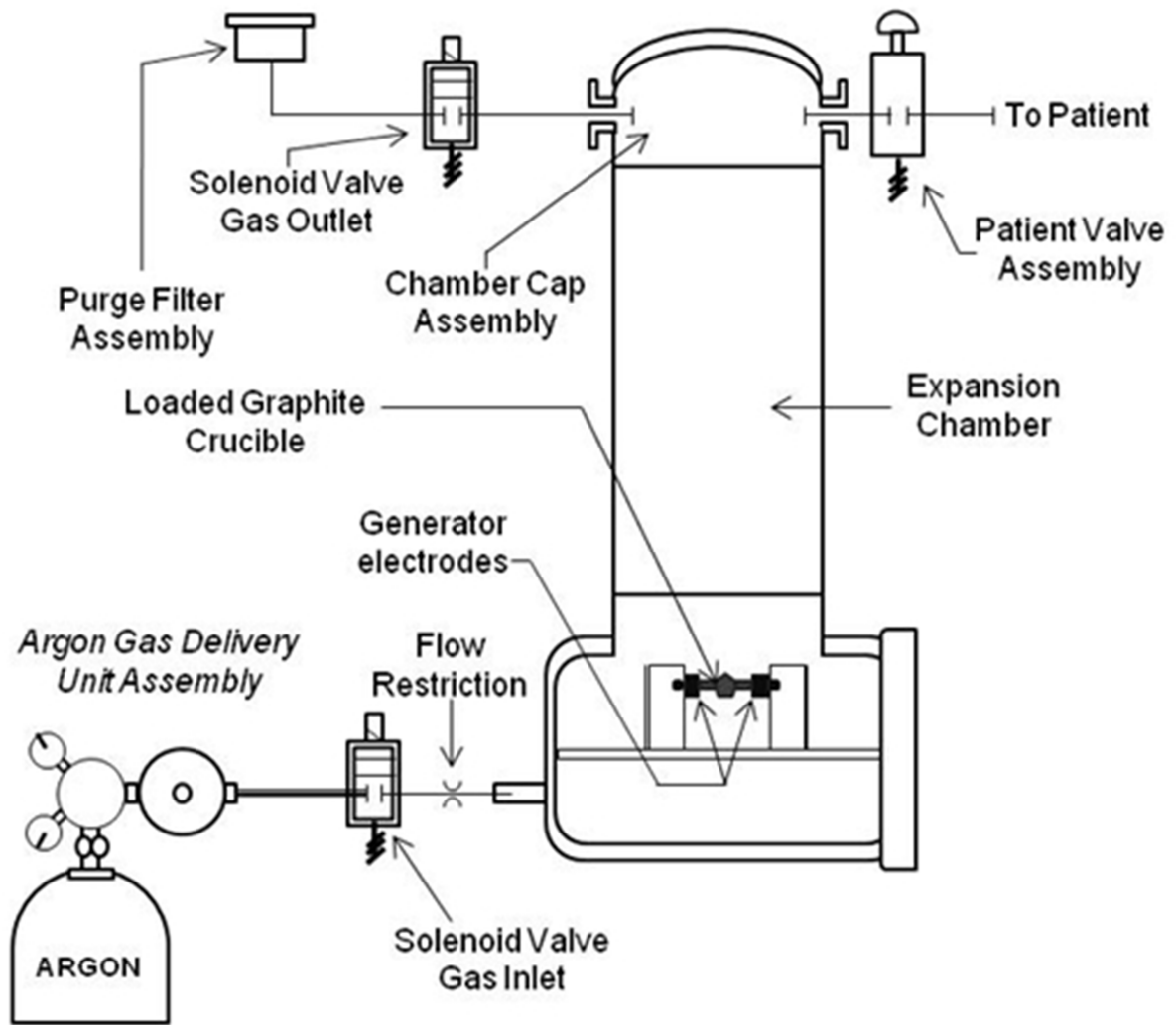
470 **FIGURE 8.** Total radioactivity of evaluated radio-aerosols: influence of operating  
471 parameters ( \* : Values are not significantly different,  $p < 0.05$ ).

472 **FIGURE 9.** Technegas aerodynamic particle size distribution: comparison between  
473 standard clinical production, optimized production and optimized production using  
474 NaCl free-eluate.

475



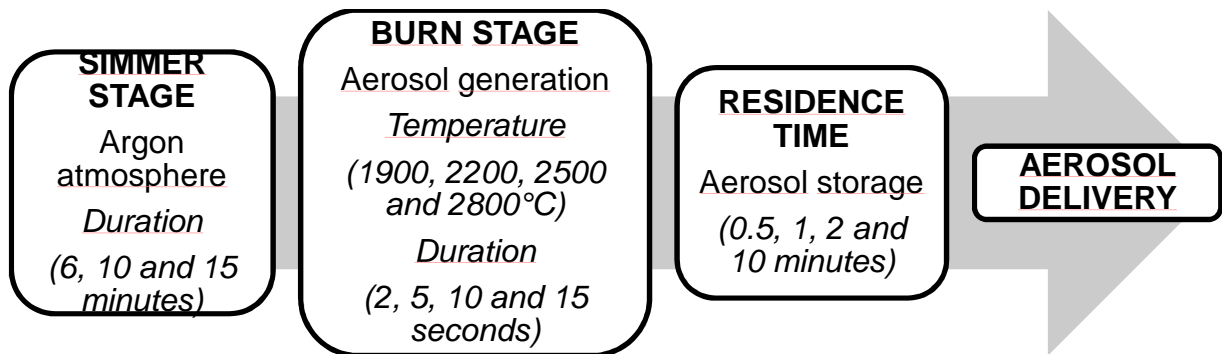
1 **FIGURE 1.** Schematic diagram of the Technegas generator.



2

3

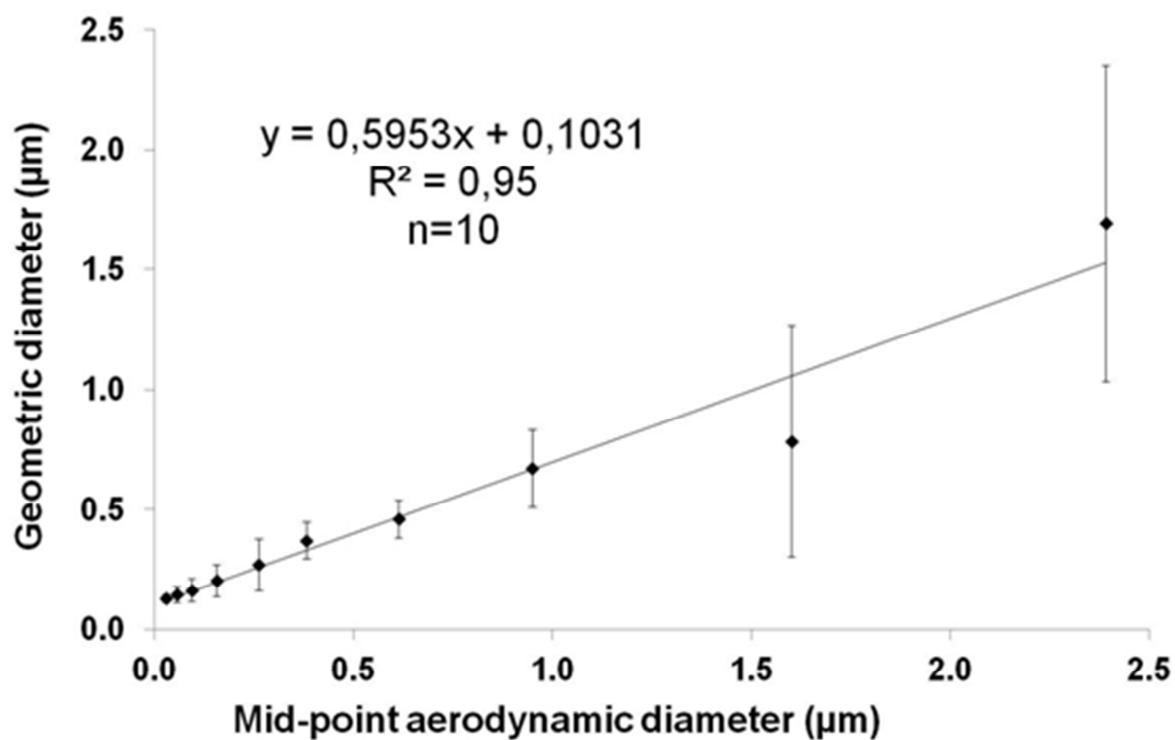
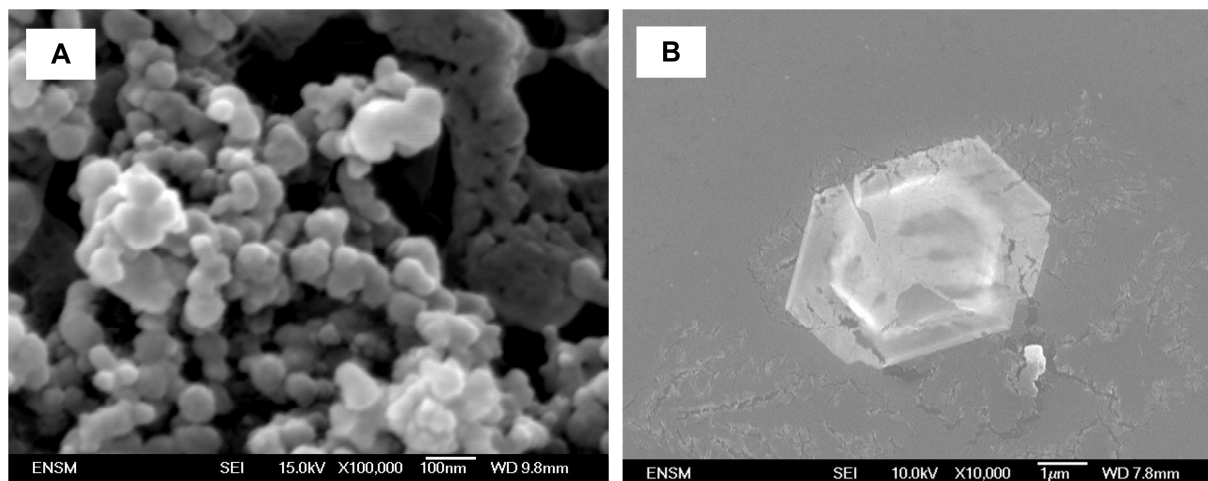
4 **FIGURE 2.** Operating conditions of the Technegas generator in the maintenance  
5 mode : description of analyzed parameters.



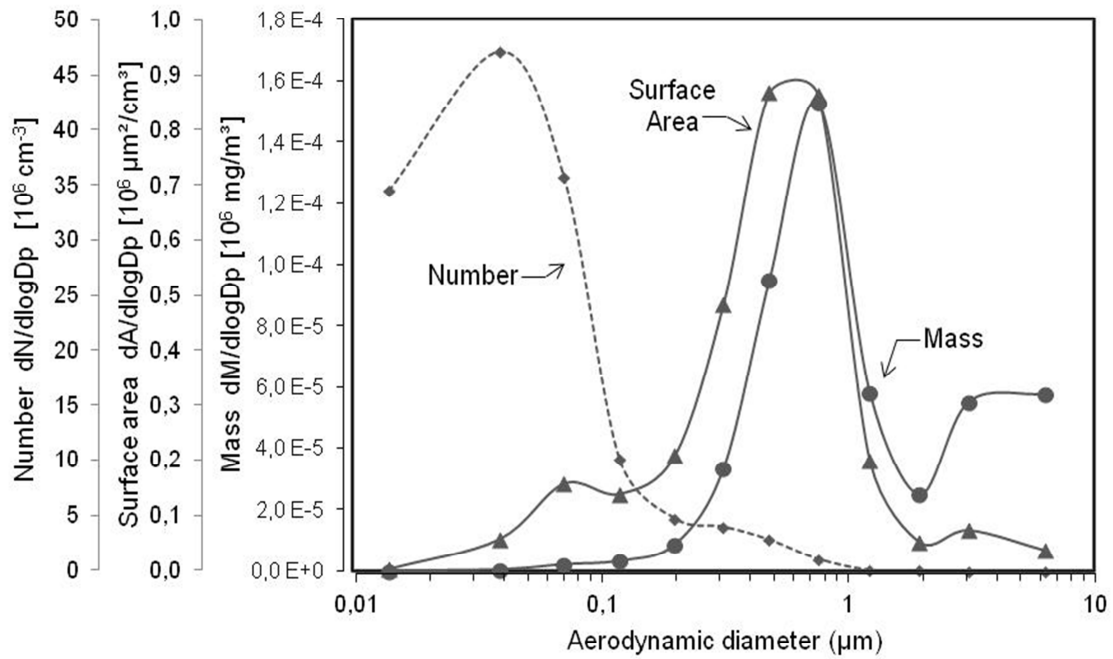
6

7

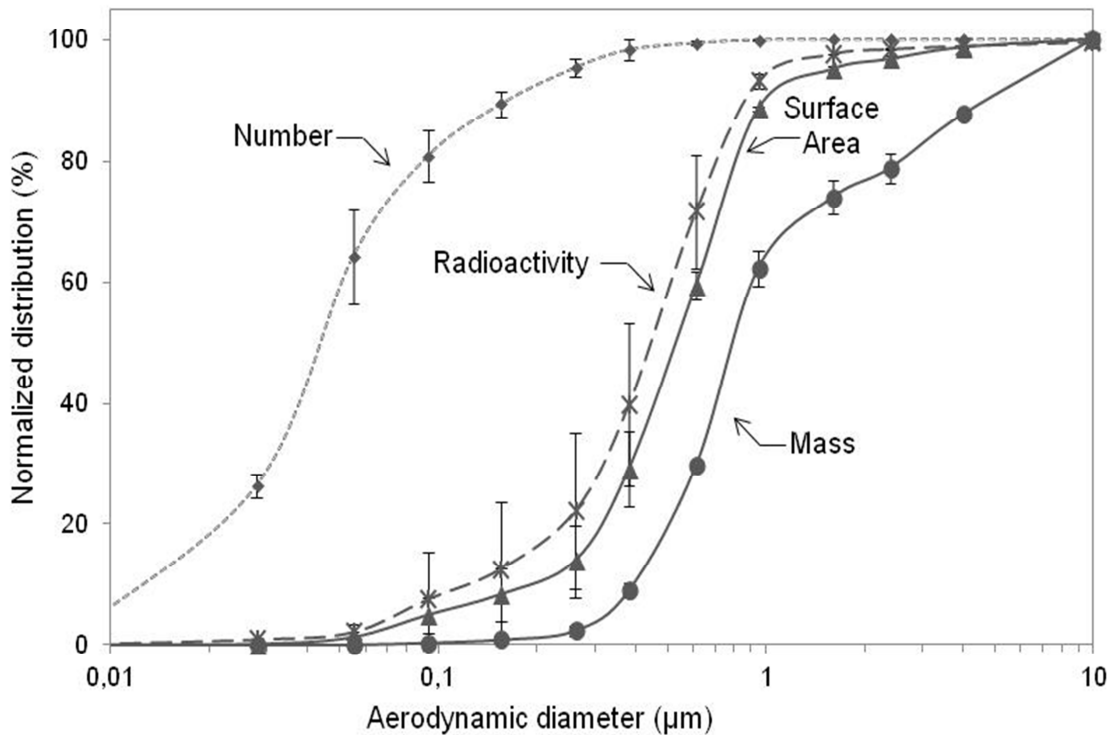
8 **FIGURE 3.** EDX analysis coupled with SEM observation of ELPI stage showing  
9 carbonaceous nanoparticles (A) and NaCl crystals (B). Linear correlation between  
10 geometric diameter obtained by image analysis on SEM images and corresponding  
11 mid-point aerodynamic diameter determined by ELPI.



15 **FIGURE 4.** Aerodynamic size distributions of aerosol generated under standard  
 16 clinical operating mode: differential distributions from ELPI calculations (top) and  
 17 cumulative distributions from combined ELPI and gamma-camera measurements  
 18 (bottom).

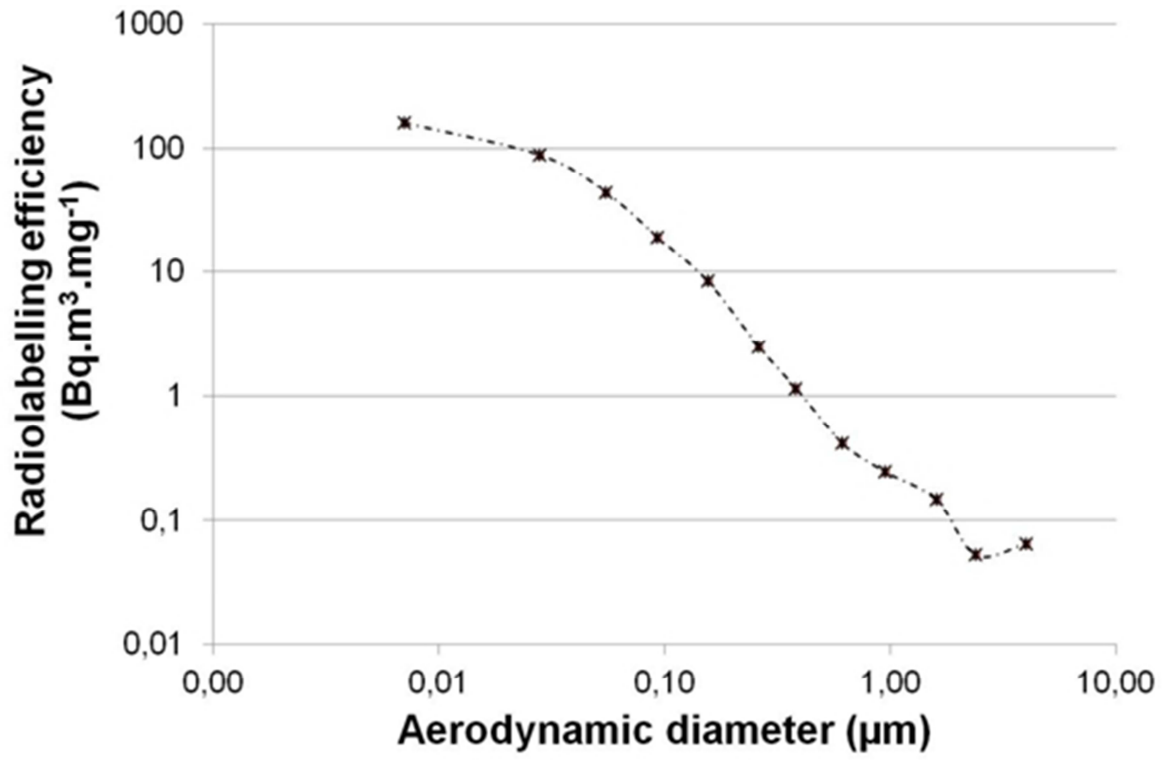


19



20

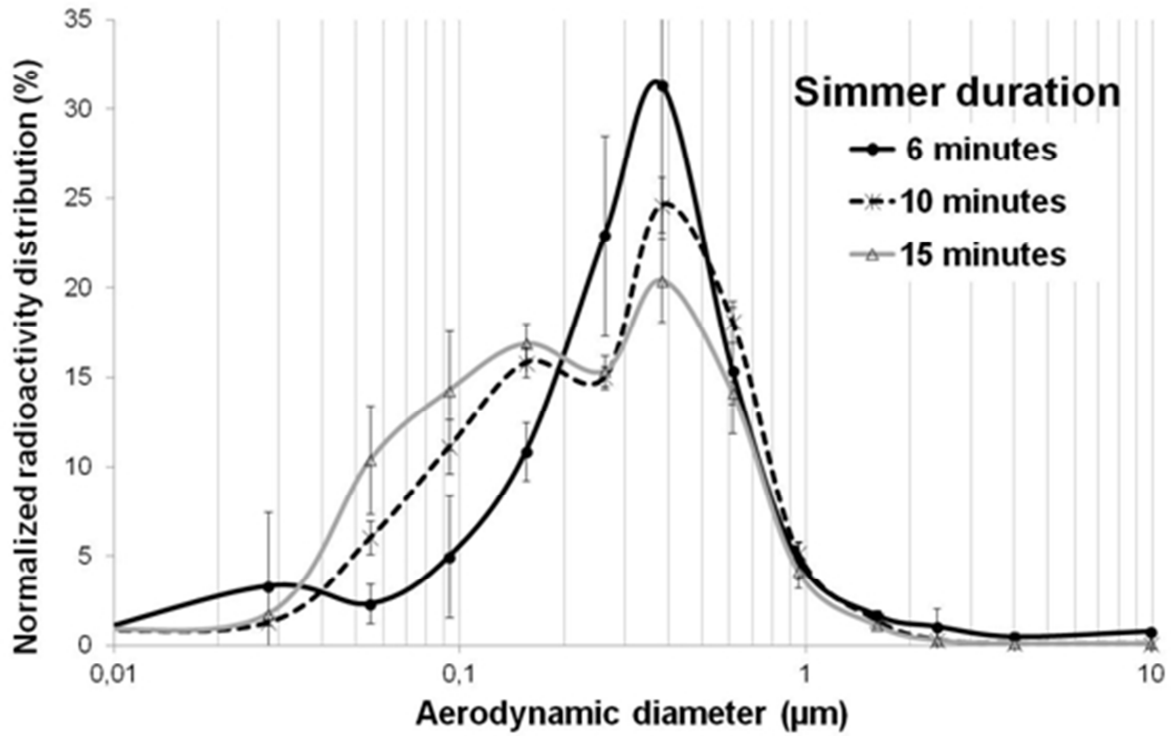
21 **FIGURE 5.** Radiolabelling efficiency expressed as activity per particle mass.



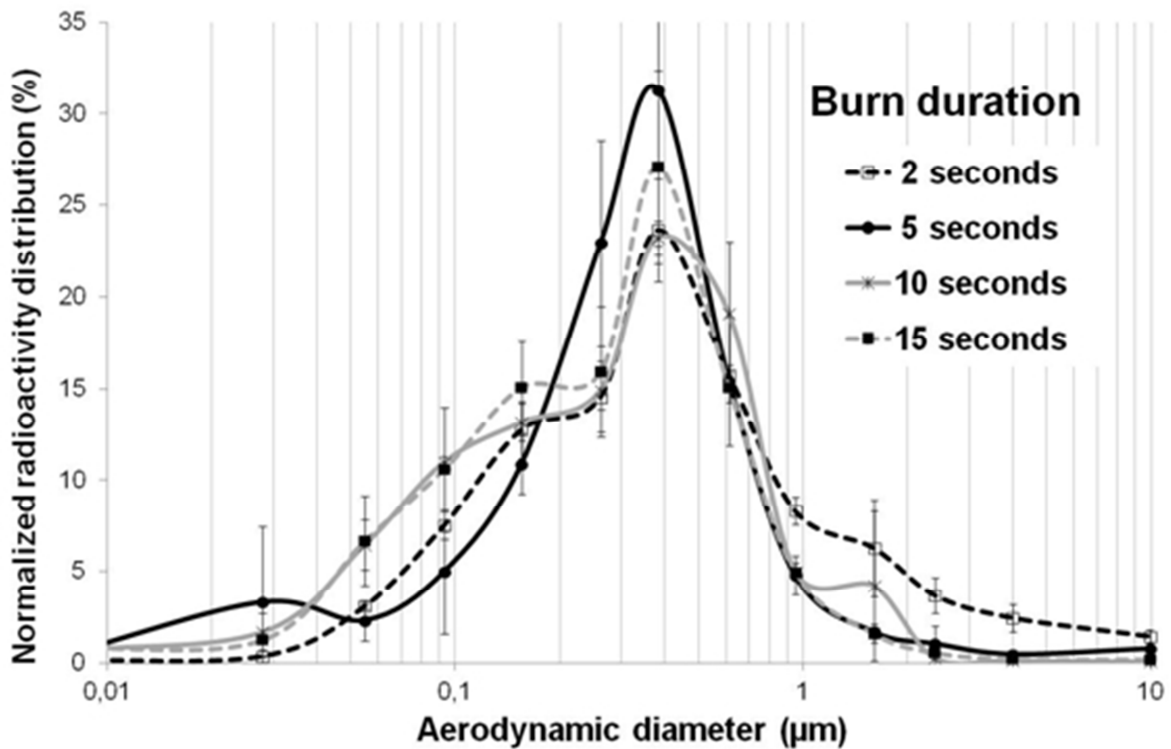
22

23

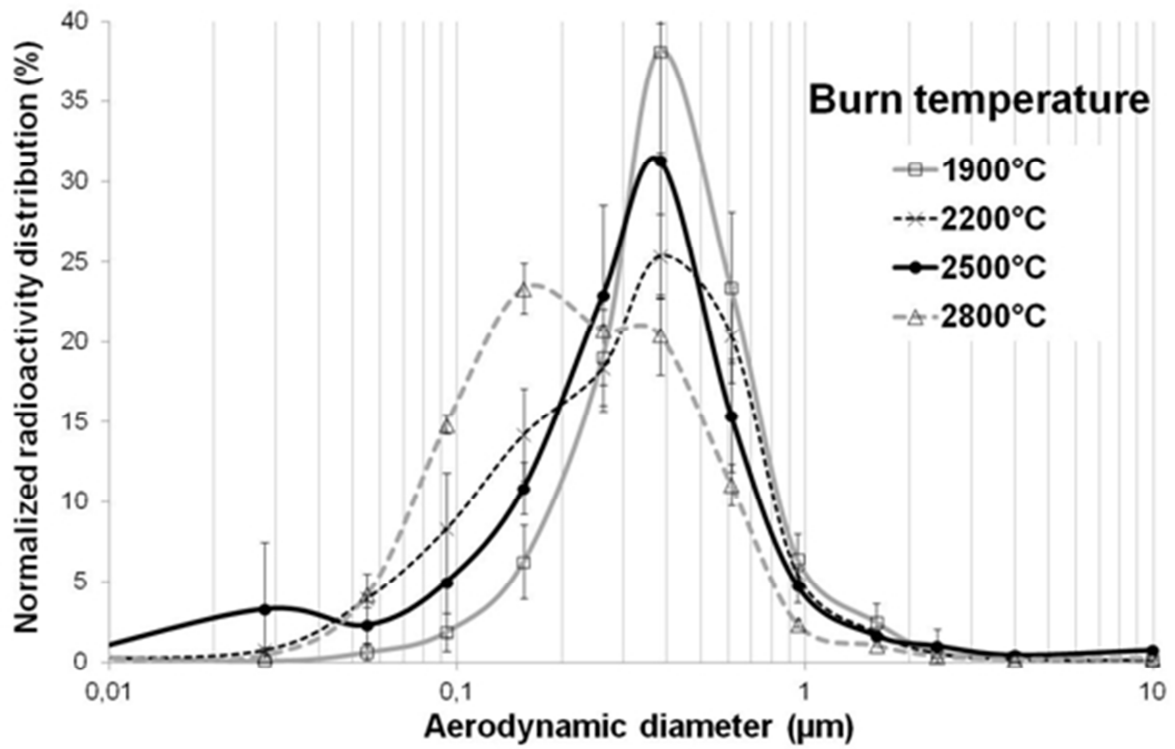
24 **FIGURE 6.** Operating parameters influencing Technegas aerodynamic particle size  
25 distribution. Clinical operating conditions are used as a reference (distribution in black  
26 bold line).



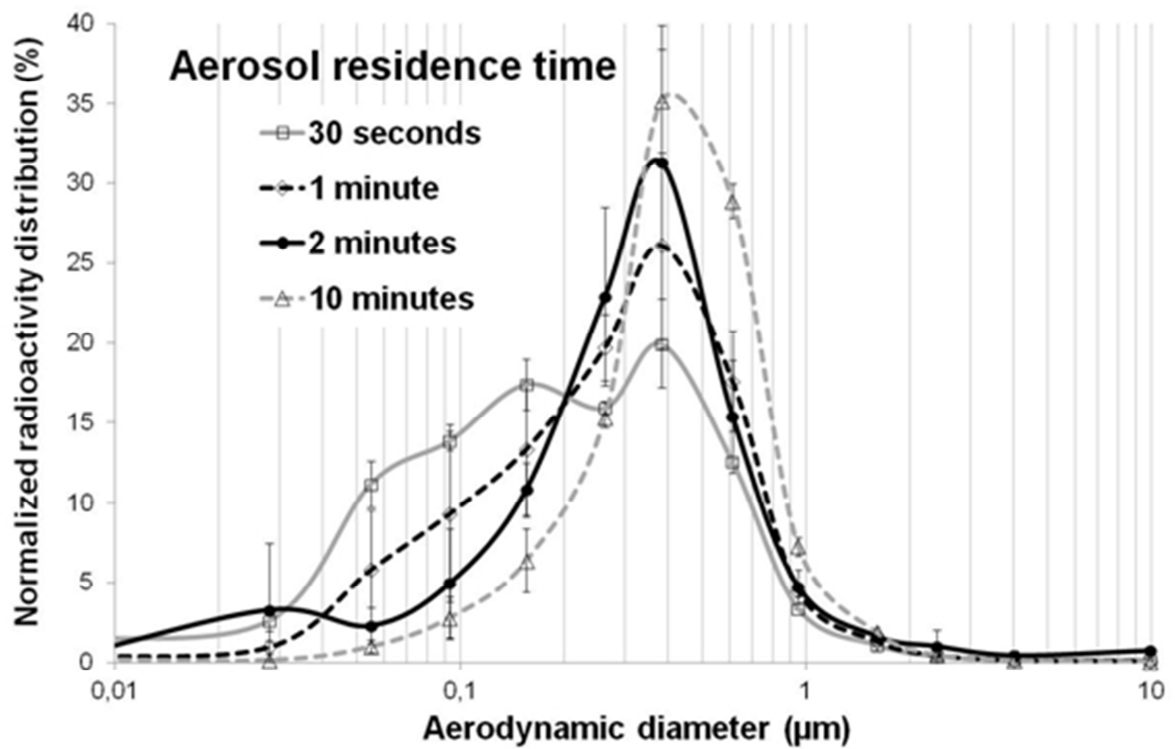
27



28



29

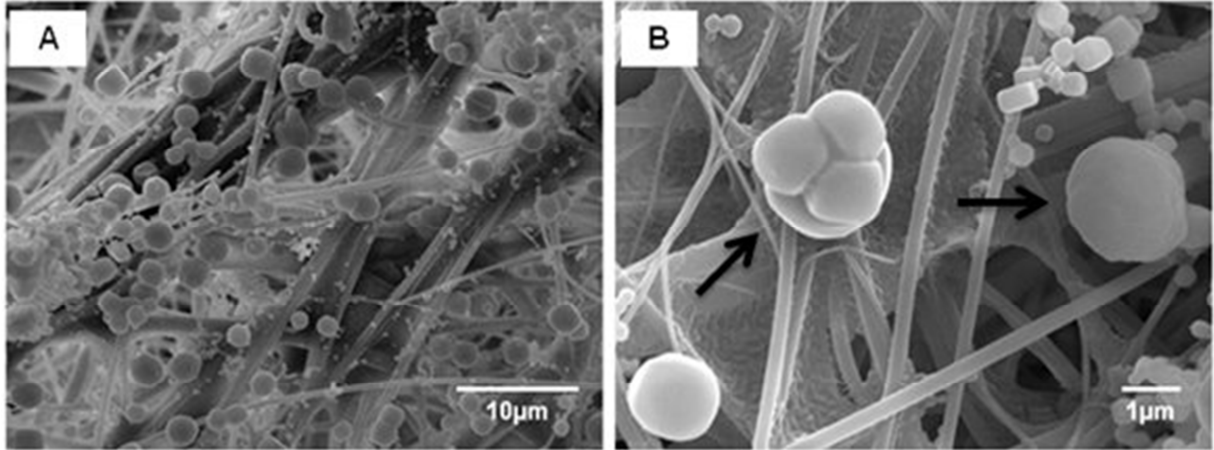


30

31

32

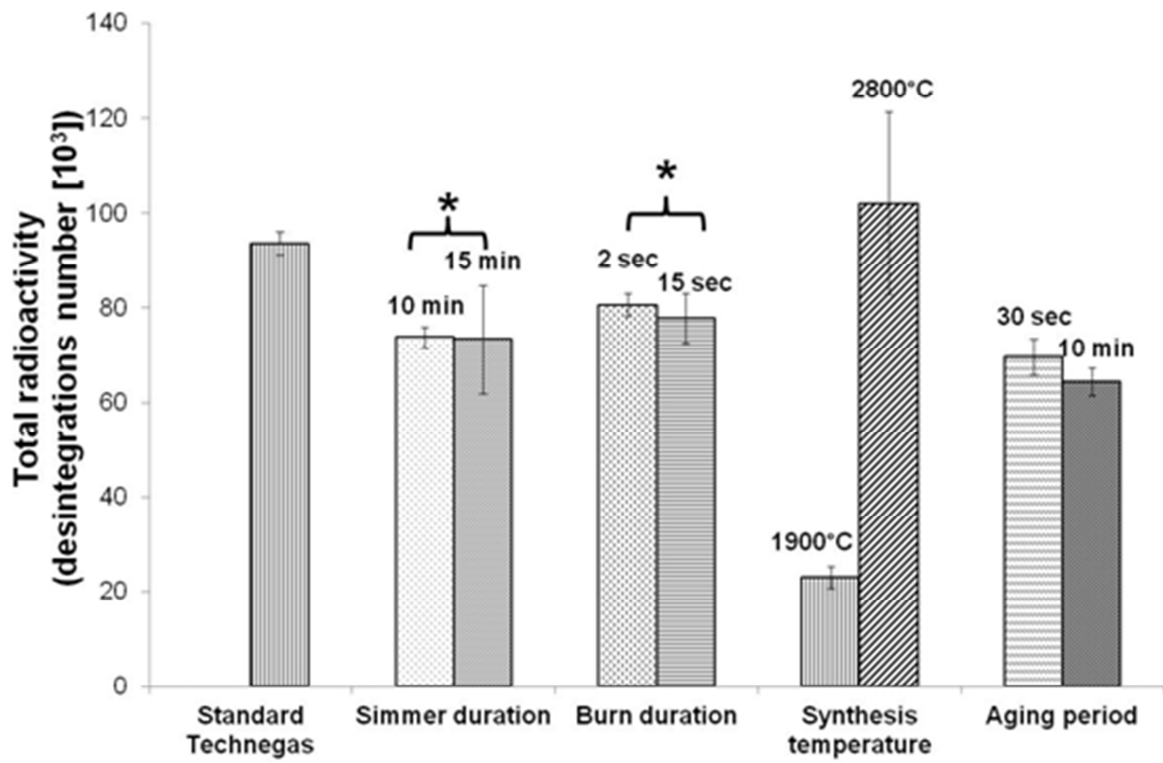
33 **FIGURE 7.** SEM images of particles deposited on ELPI stage corresponding to mid-  
34 point aerodynamic diameter of  $2.39\ \mu\text{m}$  for residence times of (A) 30 seconds and (B)  
35 10 minutes. Arrows indicate agglomerated particles.



36  
37



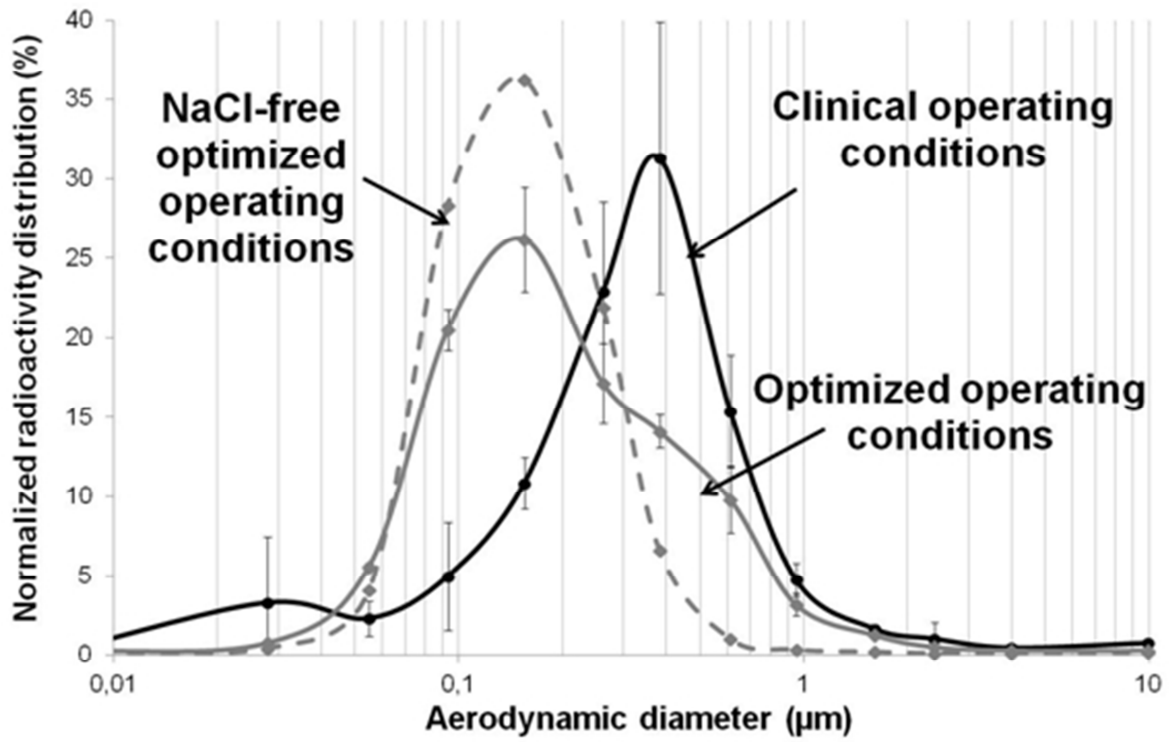
38 **FIGURE 8.** Total radioactivity of evaluated radio-aerosols: influence of operating  
39 parameters (\* : Values are not significantly different,  $p < 0.05$ ).



40

41

42 **FIGURE 9.** Technegas aerodynamic particle size distribution: comparison between  
43 standard clinical production, optimized production and optimized production using  
44 NaCl free-eluate.



45

**TABLE 1.** Influence of ELPI collection substrates on aerosols particle size distributions: radioactivity median aerodynamic diameters (AMAD) and geometric standard deviation (GSD).

Generation Mode	ELPI Measurements	AMAD (nm)	GSD
<i>standard clinical operating conditions</i>	<i>without collection substrates</i>	450*	3.4
	<i>with collection substrates</i>	445*	3.0

\* : values are not significantly different ( $p < 0.05$ )

**TABLE 2.** Radioactivity median aerodynamic diameters (AMAD) and geometric standard deviation (GSD) under standard clinical operating conditions, or under modified and optimized operating conditions (modified generation parameters in bold).

Analyzed parameters	Generation parameters				Particle size distribution	
	Simmer duration (min)	Burn duration (s)	Synthesis temperature (°C)	Residence time (min)	AMAD (nm)	GSD
<i>Standard</i>	6	5	2500	2	450	2.7
<i>Simmer duration</i>	<b>10</b>	5	2500	2	380*	2.1
	<b>15</b>	5	2500	2	305	2.2
<i>Burn duration</i>	6	<b>2</b>	2500	2	500	3.2
	6	<b>10</b>	2500	2	385*	2.5
	6	<b>15</b>	2500	2	370	2.9
<i>Synthesis temperature</i>	6	5	<b>1900</b>	2	510	3.0
	6	5	<b>2200</b>	2	420	2.5
	6	5	<b>2800</b>	2	270	2.7
<i>Residence time</i>	6	5	2500	<b>0.5</b>	285	2.8
	6	5	2500	<b>1</b>	380*	2.5
	6	5	2500	<b>10</b>	540	2.6
<i>Optimized</i>	6	10	<b>1900°C followed by 2800°C</b>	2	250	2.5

\* : values are not significantly different (p<0.05)